Published in final edited form as:
Clin Biomech (Bristol, Avon). 2014 March ; 29(3): 336–349. doi:10.1016/j.clinbiomech.2013.12.014.

An animal model to evaluate skin-implant-bone integration and gait with a prosthesis directly attached to the residual limb

Brad J Farrell[1], **Boris I Prilutsky**[1,*], **Robert S Kistenberg**[1], **John F Dalton IV**[2], and **Mark Pitkin**[3,4]

[1]School of Applied Physiology, Center for Human Movement Science, Georgia Institute of Technology, Atlanta, GA, USA

[2]Georgia Hand Shoulder Elbow, Atlanta, GA, USA

[3]Tufts University School of Medicine, Boston, MA, USA

[4]Poly-Orth International, Sharon, MA, USA

Abstract

Background—Despite the number of advantages of bone-anchored prostheses, their use in patients is limited due to the lack of complete skin-implant integration. The objective of the present study was to develop an animal model that would permit both detailed investigations of gait with a bone-anchored limb prosthesis and histological analysis of the skin-implant-bone interface after physiological loading of the implant during standing and walking.

Methods—Full-body mechanics of walking in two cats was recorded and analyzed before and after implantation of a percutaneous porous titanium pylon into the right tibia and attachment of a prosthesis. The rehabilitation procedures included initial limb casting, progressively increasing loading of implant, and standing and locomotor training. Detailed histological analysis of bone and skin ingrowth into implant was performed at the end of the study.

Findings—The two animals adopted the bone-anchored prosthesis for standing and locomotion, although loads on the prosthetic limb during walking decreased by 22% and 62%, respectively, 4 months after implantation. The animals shifted body weight to the contralateral side and increased propulsion forces by the contralateral hindlimb. Histological analysis of the limb implants demonstrated bone and skin ingrowth.

Interpretation—The developed animal model to study prosthetic gait and tissue integration with the implant demonstrated that porous titanium implants may permit bone and skin integration and prosthetic gait with a prosthesis. Future studies with this model will help optimize the implant and prosthesis properties.

Keywords

Porous percutaneous titanium implant; skin-implant-bone interface; bone-anchored prostheses; histology; prosthetic gait; osseointegration

*Corresponding Author: Boris I. Prilutsky, School of Applied Physiology, Georgia Institute of Technology, 555 14th Street NW, Atlanta, GA 30332-0356, USA, Phone: +1-404-894-7659, boris.prilutsky@ap.gatech.edu.

1. Introduction

Several types of bone-anchored (or osseointegrated) limb prostheses have been developed and evaluated in individuals with amputation (Rancho Los Amigos Hospital Implantation System (Mooney et al., 1977), Osseointegrated Prostheses for Rehabilitation of Amputees (Hagberg and Branemark, 2009), Endo-Exo Femoral Prosthesis (Aschoff et al., 2010), Intraosseous Transcutaneous Amputation Prosthesis (Pendegrass et al., 2006a)) and in animal studies (Percutaneous Osseointegrated Prosthesis (Shelton et al., 2011), Skin and Bone Integrated Prosthesis (Pitkin et al., 2006), University of Akron System (Saunders et al., 2012)). These prostheses are rigidly attached to the bone via a solid titanium implant in the marrow cavity and protrude through the skin (Branemark, 1983). Prostheses with a direct skeletal attachment (DSA) eliminate limitations of traditional socket prostheses including difficulties fitting the socket onto the residual limb, discomfort and pain due to skin irritation, development of pressure sores, sitting discomfort, limited range of motion, and transmission of external loads to the limb via soft tissues (Hagberg et al., 2005; Pezzin, 2004). In addition, the conventional socket prostheses provide little or no normal proprioceptive feedback thus, visual feedback with a relatively long delay becomes critical for successful performance of complex motor tasks (Barnett et al., 2013; Glencross, 1977). The lack of normal sensory feedback from the residual limb affects the control of balance and placement of the sound and prosthetic foot during standing and locomotion particularly on complex terrains (Buckley et al., 2002; Curtze et al., 2011, 2012; Hof et al., 2007; Segal et al., 2010). DSA prostheses might have certain advantages over traditional socket prostheses during standing and locomotion: (i) ground reaction forces are transmitted directly to the bone of the residual limb compared to indirect force transmission through soft tissues and (ii) the amputee has a better sense of load on and position of the prosthesis due to osseoperception (Jacobs et al., 2000).

Despite the number of advantages of DSA prostheses, their use in many countries, including the US, is limited or prohibited due to the lack of complete skin-implant integration. As a result amputees with DSA prostheses have a rather high skin infection rate (13%–30% (Aschoff and Juhnke, 2012; Aschoff et al., 2010), 18%–23% (Hagberg and Brånemark, 2009; Tillander et al., 2010)), which can lead to implant loosening, revision and/or removal. The majority of current DSA prostheses utilize intramedullary titanium implants with a solid percutaneous portion that has a smooth or partially modified surface (Aschoff et al., 2010; Hagberg and Brånemark, 2009; Jonsson et al., 2011). Since solid percutaneous implants do not completely eliminate skin infection problems, researchers have tried to improve the skin-implant integration through the use of porous implants (Pitkin et al., 2004; Pitkin et al., 2006), or implants with perforated flange, imitating natural percutaneous structures such as the deer antler (Pendegrass et al., 2006c). Recent *in vitro* and *in vivo* studies of porous implants have demonstrated a potential for a better skin-implant integration and the possibility of developing a robust skin barrier to bacteria and other pathogens (Chou et al., 2010; Farrell et al., 2013b; Jeyapalina et al., 2012; Pendegrass et al., 2006b; Pendegrass et al., 2008; Pitkin et al., 2006; Pitkin et al., 2007; Pitkin et al., 2009; Shelton et al., 2011).

Gait analysis in individuals with amputation who have prostheses directly attached to their residuum, has had the following principle aims (D'Angeli et al., 2013; Frossard et al., 2009; Frossard et al., 2010b; Frossard et al., 2013; Frossard et al., 2008a; Frossard, 2010; Frossard et al., 2010c; Isackson et al., 2011; Lee et al., 2007; Lee et al., 2008; Tranberg et al., 2011; Van de Meent et al., 2013): to optimize the mechanical design of the fixation, to refine the rehabilitation program, to compare the performance of the osseointegrated prostheses with socket prostheses, to evaluate walking ability, effect of falls and prosthetic components. Such gait studies have been conducted with the two commercially available DSA systems: OPRA - Osseointegrated Prosthesis for the Rehabilitation of Amputees (Brånemark et al.,

2001) and EEFP/ILP - Endo - Exo-Femur Prosthesis/Integral Leg Prosthesis (Aschoff et al., 2010). As new experimental DSA systems emerge (Pitkin, 2013), a need exists for adequate animal models, which through gait studies will help in selecting the best technologies without compromising the safety of human subjects.

The effects of porous or porous-coated implant properties on skin and bone integration have been studied in animal models: rats (Ysander et al., 2001), guinea pigs, rabbits (Jansen and de Groot, 1988; Jansen et al., 1994; Pitkin et al., 2006), cats (Pitkin et al., 2009), dogs (Drygas et al., 2008; Murphy, 1973), pigs (Fernie et al., 1977), goats (Hall, 1974) and sheep (Shelton et al., 2011; Williams et al., 2010); with few of these studies involving any gait analysis. A recent study in sheep showed that loading on the implanted limb decreased to approximately 74% of the pre-implantation load 12 months after implantation of a percutaneous osseointegrated prosthesis with porous skin-implant interface into third metacarpal bone (Shelton et al., 2011). The limited data on reduced load on DSA prostheses attached through porous percutaneous implants during gait might indicate potential problems with integration between the implant and residual limb. This warrants further investigation and development of an animal model that permits detailed histological investigations of skin and bone integration, as well as detailed biomechanical analysis of gait with DSA prostheses.

A feline model appears to be well suited for this purpose. It has been the model of choice in studies of the neural control and biomechanics of posture and locomotion (Beloozerova et al., 2010; Brown, 1914; Honeycutt and Nichols, 2010; Musienko et al., 2012; Rossignol, 2006; Sherrington, 1910; Shik et al., 1966). The advantage of the cat model compared to a rodent model is that the cat has highly developed locomotor abilities, it maintains the upright posture, and the loads experienced by the hindlimbs during locomotion are larger than those in rodents and have similar patterns to human ground reaction forces during walking. Loading on the implant is especially important because the degree of osseointegration has been shown to be load dependent (Torcasio et al., 2008). Furthermore, cat limb inertial properties have been determined (Hoy and Zernicke, 1985), which permits calculations of forces and moments at the joints and the prosthesis interface with the residual limb by means of inverse dynamics analysis (Gregor et al., 2006; Hoy and Zernicke, 1985; Manter, 1938; Prilutsky et al., 2005). Larger animal models (e.g., large dogs, sheep) have also been used to study DSA prostheses (Shelton et al., 2011), however lab settings for a detailed biomechanical analysis of prosthetic gaits in these models are not readily available.

The objective of the present study was to develop a feline prosthetic gait model for evaluating locomotion with the DSA prostheses attached via porous titanium implants (Farrell et al., 2013b; Pitkin et al., 2009) and for testing skin-implant-bone integration of these implants. This model would permit both a detailed histological analysis of the skin-implant-bone interface after physiological loading of the implant during standing and walking and investigations of prosthetic gait adaptations. Based on data available (Farrell et al., 2013b; Jeyapalina et al., 2012; Pitkin et al., 2007; Pitkin et al., 2009; Shelton et al., 2011) we hypothesize that (1) the animals will adopt the prosthesis for standing and walking, although gait mechanics would change and (2) skin and bone tissue will be present inside the porous titanium implants after mechanical loading of implant during normal physiological activities such as standing and walking. The preliminary results of the study have been published in abstract form (Farrell et al., 2012; Farrell et al., 2013a).

2. Methods

2.1. Animal model and study design

All experimental procedures in this study were in agreement with the US Public Health Service Policy on Humane Care and Use of Laboratory Animals and were approved by the Institutional Animal Care and Use Committees of Georgia Institute of Technology and Saint Joseph's Translational Research Institute. Two adult purpose bred cats (mass 3.2 and 3.0 kg) were selected for this study. They were trained daily for two weeks to walk across an enclosed walkway with embedded force platforms for food reward. After completion of training, full body walking mechanics were recorded (see section 2.8) for another two weeks (for time line of study see Figure 1A). X-ray images were taken prior to surgery to measure the dimensions and geometry of the tibia marrow cavity, and after implantation to monitor healing and possible bone lysis or fracture (Figure 1B). After implantation of the implant into the tibia medullary cavity (see below), a cast was placed on the residual limb to prevent premature loading of the implant (Figure 1B, C). Starting at week 6 after implantation, the protruding end of implant was progressively loaded (Figure 1D) to promote bone-implant integration (Frossard et al., 2008b; Torcasio et al., 2008). At the end of week 10 the cast was removed and a standing prosthesis (Figure 2A) was attached to the protruding implant 2–3 times a day to train the animal to use the prosthesis for standing. After initial training for 1 week, the animals started wearing the standing prosthesis continuously. Starting at week 12–14, a J-shape walking prosthesis was attached (Figure 2B, C), and the animals were retrained to walk along the walkway using food reward. Training lasted for 4–6 weeks until the animals started repeatedly crossing the walkway (at least 15–20 times in a recording session) with loading the prosthetic leg. Walking mechanics were recorded for several weeks. At week 21 the animals were euthanized using deep anesthesia and the limb with implant was harvested for histological analysis (see section 2.9).

2.2. Implants

Porous titanium implants were obtained from Poly-Orth International (Sharon, MA, USA). The manufacturing technology for these implants has been described elsewhere (e.g. (Farrell et al., 2013b; Pitkin et al., 2012; Pitkin and Raykhtsaum, 2012; Pitkin et al., 2009)). Implants were tapered to fit the tibia marrow cavity (0.3 cm diameter at proximal end × 0.5 cm diameter at distal end × 5 cm in length; Fig. 1B) and had a central 0.3 × 0.3 cm cross-shaped titanium rod. Pore size in the implant ranged from 40–100 μm (porosity of 30–50%). The distal 0.7 cm of the implant had no porous coating and served as the prosthesis attachment interface.

2.3. Implantation surgery

After cats were trained and pre-implantation gait mechanics were recorded (see section 2.8), each cat underwent an amputation and implantation surgery using standard aseptic surgical procedures. Animals were sedated and pre-anesthetized using a combination of drugs (Dexmedetomidine, SC, 60–80 μg/kg, Ketamine, SC 10 mg/kg, and Xylazine, SC, 10 mg/kg) and anesthesia was maintained using isoflurane inhalation, 1–3%). The right hindlimb was shaved and scrubbed. A circumferential incision was made at the level of the distal ⅓ of the tibia. In making this incision, a posterior skin flap was incorporated to allow for tension-free closure. The muscles and tendons at this level were transected using electrocautery. The periosteum was reflected from the exposed tibia proximal to the level of the skin incision and a transverse osteotomy was performed at the juncture of the middle and distal thirds of the tibia using an oscillating saw. The edges of the tibia were rasped to eliminate any sharp edges. A fibular osteotomy was performed approximately 2 cm proximal to the level of the tibial osteotomy. Any remaining soft tissue was transected using cautery thereby completing the amputation. The medullary canal of the tibia was broached using a curette and carefully

widened with a reamer that had the same diameter and taper as of the implant. Prior to closure, the fat and subcutaneous tissue of the posterior skin flap was sharply excised to the level of the dermis. A small stab incision was placed with a 15 blade through the posterior skin flap. The sterile implant was inserted through this incision and into the medullary canal of the tibia to a depth of approximately 2–3 cm. The wound was copiously irrigated with normal saline and closed with nylon suture so that the dermis of the posterior skin flap made direct contact with the distal end of the tibia. These procedures allowed for a tight interface between the skin and the implant as well as the skin and bone. A sterile gauze dressing was applied over the pylon through a hole placed in the gauze in order to further secure the skin-implant-bone interface. Additional gauze dressing was applied around the pin with sufficient bulk to protect and pad the implant.

The limb was then casted from the proximal thigh to just past the distal end of the implant using a modified Robert Jones Bandage (Brodell et al., 1986) (Figure 1C) to protect the implant and prevent premature loading. In summary, tape stirrups running down the medial and lateral aspects of the limb were used to secure the cast. A nylon stocking was placed over the leg for casting followed by layers of cast padding and roll gauze. Fiberglass casting tape (Scotchcast, 3M, USA) was applied to the limb. The distal portion of the cast was covered with a ventilated small plastic jar and a screw cap that allowed access to the implant. The jar and screw cap were secured to the cast using vet-wrap (3M). The animal recovered for 1–2 weeks with the pain medication administered for at least 3 days and antibiotics for at least 10 days. Blood samples were taken once before surgery and then one week after the surgery to monitor white blood cells counts and infection. Body temperature was measured for several weeks after surgery.

2.4. X-ray

Prior to the implantation surgery sagittal and frontal plane X-ray images of the right tibia were taken (Figure 1B). The images aided in determining geometry and dimensions of the tibia marrow cavity, surgical planning and implant selection. After implantation surgery, X-ray images were taken every two weeks (or as needed) to monitor healing and possible bone lysis, fracture and implant loosening.

2.5. Implant loading

Six weeks after implantation, each cat was gently restrained, fed and petted by a researcher while another researcher removed the distal cast cover. An axial force of 1.2 N was applied to the distal end of the implant (for 15 minutes a day, 3 days a week) using the digital dynamometer. Each week the load was increased by 3.1 N to reach in 4 weeks 13.6 N (Figure 1D), i.e., the load close to the peak vertical force exerted by the hindlimb during walking or 40–50% of animal body weight. The above implant loading procedure is a scaled version of the procedure used to promote osseointegration of implant in human amputees (Aschoff et al., 2010; Frossard et al., 2010a; Frossard et al., 2008b; Hagberg and Brånemark, 2009). The initial load in our study (4% of body weight) was lower than used in human amputees (25%) to avoid or minimize potential pain, the weekly load increase was comparable (10% vs. 12% in humans) and the final load magnitude corresponded to the peak vertical ground reaction force during walking in agreement with rehabilitation procedures in humans (Hagberg and Branemark, 2009; Sullivan et al., 2003).

2.6. Prostheses

Once the loading of the implant achieved 40–50% of body weight (approximately 10 weeks after implantation), the restraining cast was removed and a prosthesis was attached to the skin-protruding part of the implant (approximately 2 cm in length) through a female receptacle and setscrews (Figure 2A, B). The first prosthesis attached was a standing

prosthesis made of an aluminum rod (9 cm diameter × 6.5 cm length) milled to fit a non-slip rubber tread mounted to the bottom (Figure 2A). The animals were adapted to standing on this prosthesis for several weeks before a walking prosthesis was attached.

The walking, J-shape prosthesis incorporated a rocker bottom (Figure 2B, C) to simulate foot-paw function during walking. The curved portion of the prosthesis was fabricated using molded carbon fiber. A hook and loop strip were attached to the bottom of the foot so that treads with different thickness and friction coefficient could be exchanged easily without changing the prosthesis. The initial prosthesis design (length and curvature) was selected to match intact hindlimb length at touch down, mid-stance and lift-off assuming that hip and knee angles would remain unchanged. Prosthesis curvature and length were adjusted as needed to improve symmetry of prosthesis loading and gait speed.

The inertial parameters of each prosthesis were determined for subsequent prosthetic gait analysis (Table 1). The mass was measured using a digital scale and the location of the center of mass in the sagittal plane (Figure 2A, B; red dots) was determined using a suspension method (e.g., (Drillis et al., 1964)). The moment of inertia with respect to the frontal axis through the center of mass was calculated using measured elemental areas of the prosthesis from its high resolution image and known material density of each elemental area; the computed moment of inertia was compared to a computer generated moment of inertia (SolidWorks, Dassault Systèmes, MA, USA).

2.7. Rehabilitation procedures

Initial wearing time for the standing prosthesis began with 20 minutes, twice a day and the wear time increased gradually so that the cats could continuously wear the prosthesis by the end of the first 1–2 weeks after cast removal. Cats were initially trained to stand on the prosthesis using food reward. During training cats were fed when they successfully stood on the prosthetic limb. Standing training continued daily for 1–3 weeks.

After adequate standing was achieved, cats were transitioned to the walking, J-shape prosthesis. They were trained for several weeks to walk and stand on the new prosthesis. Positive reinforcement (petting and food) was used when the cats would demonstrate loading of the prosthesis during walking. Once the researchers deemed the cat reached consistent walking performance on the prosthesis (repeated crossing the walkway with loading the prosthetic leg), gait recording commenced.

2.8. Gait recordings and analysis

Full-body mechanical characteristics of intact and prosthetic gait were recorded before surgery and after rehabilitation. In each experimental session, 28 small reflective markers (6–9-mm in diameter) were attached to major joints and body segments on the cat and/or prosthesis using double-sided adhesive tape (Figure 2D). Three-dimensional marker positions and the three components of the ground reaction force were recorded using a high-speed motion capture system (120 Hz; Vicon, UK) and 3 force plates embedded in the walkway (360 Hz; Bertec, USA). The walkway (3 m × 0.4 m) allowed for recordings of 2–5 consecutive strides by each limb depending on locomotion speed. Food reward was given each time the cat successfully walked across the walkway. Gait mechanics were recorded daily for approximately 3–5 weeks.

Gait mechanics were analyzed using a full-body inverse dynamics cat model (see Fig. 2D and (Beloozerova et al., 2010; Farrell et al., 2013a; Prilutsky et al., 2005)). In summary, recorded trials were examined for consistent walking with constant velocity. The marker positions were low-pass filtered (Butterworth, zero lag 4^{th} order filter, cutoff frequency 6–7Hz). For each trial, kinematics of body segments and the general center of mass (CoM)

were calculated. To compute positions of the joint centers, a limb plane was established using the hip, knee and ankle marker positions for hindlimbs or the shoulder, elbow and wrist marker positions for forelimbs (see Figure 2D; (Farrell et al., 2013a)). Within this plane, the knee and elbow marker positions were recalculated using measured limb segment lengths (Gregor et al., 2006). The estimated joint centers for the knee, ankle, elbow and wrist joints were calculated by shifting the marker positions medially half the width of the joint along the orthogonal vector to the limb plane. The hip and shoulder joint centers were estimated by shifting the marker position medially along the line defined by the left and right hip or shoulder markers half the width of the joint. The centers of mass location for each segment was calculated using the computed joint centers, the mass of the cat and the measured length of each segment (Hoy and Zernicke, 1985). The CoM displacement for each cat was determined based on the locations of each segment center of mass (e.g., (Drillis et al., 1964)). The velocity and acceleration of the CoM was calculated as the first and second time derivative of its position, respectively.

Stride kinematic parameters were calculated for each analyzed stride. Stride length was defined for all limbs as the distance between consecutive paw (or prosthesis) positions at contact with the ground. Stance width was determined for forelimbs as the lateral distance between the left and right fore paw centers, and for the hindlimbs as the lateral distance between left and right hind paw centers, or from left hind paw center to “prosthesis foot” center. Forward velocity was calculated as the mean velocity of the CoM over the gait cycle. Stance, swing and cycle times were determined based on the paw contact and lift-off times. Measured ground reaction forces and computed resultant joint moments normalized by cat body mass were time normalized and averaged across fore- or hindlimbs for each animal.

2.9. Histology

At the end of the study, animals were euthanized using deep anesthesia (an overdose of sodium pentobarbital, 120–180 mg/kg, IV) and the residual shank with implant was carefully removed by knee disarticulation. Samples were fixed in 10% neutral buffered formalin, embedded in methlymethacrylate, sectioned and ground to thickness of 100 μm using the Exakt system (EXAKT Technologies, Inc., Oklahoma City, OK, USA), then polished and stained with haemotoxylin and eosin. The samples were sectioned at the level of proximal half of implant (4 transverse sections with a step of approximately 2 mm) and at the distal end (one longitudinal section) as shown in Figure 9 A). The slides were qualitatively evaluated for tissue response and bone and skin ingrowth into implant in each section. For the purpose of scoring the degree of bone ingrowth into the porous implant at each sectioned level of the pylon, a grade 1 through 4 was assigned if bone ingrowth was observed in one, two, three or four quadrants of the porous coating, respectively. Furthermore, bone ingrowth was characterized as “superficial” when it was restricted to the outer layers or the porous structure and “deep” when the growth extended to the central rod and the inner porous coating. In addition to quantification of new bone ingrowth into the porous implant, a subjective interpretation of generalized endosteal (from inner surface of the cortical bone) and periosteal (from outer surface) bone proliferation was determined (Table 3).

2.10. Statistical Analysis

All mechanical time-dependent variables (anterior-posterior and vertical ground reaction forces and resultant muscle moments at the knee and hip of the right hindlimb before and after implantation and of the left hindlimb) were time normalized to 100% of either stance time or cycle time and averaged across all strides for each animal. Gait parameters (walking speed, stride time and length, stance time and width, duty factor) before and after surgery for each animal were compared using a Student t-test for dependent variables. The same test

was used to determine differences in time dependent variables at each percent of gait cycle between pre and post-surgery gait. Significance level was set at $P<0.05$ for all variables in the study.

3. Results

The two animals implanted with porous titanium implants did not have clinical signs of skin infection (swelling, erythema and pus (Rajan, 2012)), distress or pain, had normal temperature (range: 35.6 to 37.8 °C), white blood cells count (range: 9.5 to 11 × $10^3/\mu L$) and appetite (body mass increased after surgery from 3.2 kg to 4.0 kg and from 3.0 to 4.0 kg in cats 1 and 2, respectively). No indications of bone lysis, fracture or implant loosening could be found in X-ray images of the residual limb (Fig. 1B) for the duration of the study (20 weeks). The animals adopted the cast for standing and walking within several days after surgery (Figure 1C); subsequently (starting with week 12), the animals utilized DSA prosthesis for standing and walking.

3.1. General kinematics of prosthetic gait

Each cat successfully used the prosthesis for locomotion. Both cats tended to walk slower with the prosthesis than during intact locomotion, however only cat 1 showed significantly lower walking speed and longer cycle duration (Figure 3). Nevertheless, speed of walking with the prosthesis was within normal ranges (0.3 – 0.6 m/s (Goslow et al., 1973)). Stride length was shorter in both cats (by about 9 cm or 18%; $P<0.05$), whereas stance width was much wider (over 2 times; $P<0.05$) during prosthetic gait compared to intact walking in cat 2, but was not statistically different in cat 1. Stance time of the prosthetic right hindlimb increased in cat 1 and decreased in cat 2 by about 100 ms (~20%; $P<0.05$, Fig. 3). Duty factor during prosthetic gait tended to be higher for the intact limbs, i.e. for contralateral (left) limbs for both cats and in the ipsilateral (right) forelimb for cat 2; $P<0.05$). Duty factor for the right prosthetic limb decreased significantly in both cats.

Limb support pattern (sequence of phases with different number of limbs on the ground) showed substantial differences during prosthetic gait. Cat 1 used a limb support pattern 4-3-2-3-2-3-2-3, which was different from a pattern used in intact condition, i.e. 3-2-3-2-3-2-3-2 (Figure 4, Table 2). In this animal the most substantial difference was an increased stance contribution (duty factor) of the left hindlimb, followed by the left forelimb (Figure 3). Cat 2 used a limb support pattern (3-2-3-2-3-2-3-2) typical for moderate walking speeds (Beloozerova et al., 2010; Farrell et al., 2013a). Both cats increased the time spent in 3–4-legged support and reduced time of 2-legged support during prosthetic gait (Table 2).

The prosthetic right hindlimb demonstrated qualitatively different kinematics compared to the intact limb. The knee and hip joints of the prosthetic limb were more extended during stance and much less flexed during swing; consequently, the pelvis, thigh and the residual shank were oriented more vertically and the pelvis vertical position was higher during prosthetic walking (Figure 5).

3.2. Kinetics of prosthetic gait

During prosthetic walking, the animals loaded the prosthesis less than the intact right hindlimb prior to implantation. During intact walking, a peak vertical force on the hindlimb was 43% and 52% body weight (BW) for cat 1 and cat 2, respectively (Figures 6, 7). After surgery the prosthesis was loaded to 33% and 20% BW for cat 1 and cat 2, or 78% and 38% of the load on the same hindlimb prior to surgery. It should be noted however that in terms of absolute peak vertical forces the prosthetic limb of cat 1 was loaded similarly to load on the intact right hindlimb before surgery (13.1 N vs. 14.2 N, respectively) due to an increase

in mass of animal 1 (see above). The anterior-posterior forces on the prosthetic hindlimb also decreased in comparison with intact forces (Figures 6, 7, left panels). Specifically, the prosthetic limb of cat 1 exerted lower breaking forces for much longer time (approximately two thirds of the stance duration compared to about one third of stance in intact conditions), and produced very little propulsive force (Figure 6). Cat 2 exerted essentially no braking or propulsive forces in the anterior-posterior direction by the prosthetic limb (Figure 7).

The ground reaction forces applied to the other intact limbs during prosthetic walking demonstrated marked changes compared to intact conditions. The vertical loading of the left contralateral hind- and forelimb increased above forces in intact conditions (Figures 6, 7, right panels), while the vertical loading on the right ipsilateral forelimb remained similar or decreased slightly. The left hindlimb increased peak vertical loading by approximately 13% BW in cat 1 and 17% BW in cat 2 ($P<0.05$). The anterio-posterior forces on the intact limbs during prosthetic walking were typically lower than prior to implantation except the left contralateral hindlimb, whose breaking force was only slightly reduced, but propulsive force was higher in terminal stance ($P<0.05$, Figures 6, 7).

The resultant muscle moments at the knee and hip joints were calculated based on the ground reaction forces, limb kinematics and inertial parameters of the segments (Hoy and Zernicke, 1985) or prosthesis (Table 1). The resultant muscle moments at the hip and knee of the prosthetic limb were lower than during intact walking throughout most of the stance ($P<0.05$, Figure 8). The contralateral hindlimb, conversely, increased hip and knee moment contribution, thus providing the necessary thrust to propel the body forward.

3.3. Bone and skin integration with porous titanium implant

Histological analysis of sections through the residual limb with implant demonstrated bone ingrowth into pores of the implant in both animals, although ingrowth was not equal around the circumference of the implant and was greater in areas closer to the residual tibia (Figures 9, 10). Bone ingrowth was typically noticed in one to three quadrants of implant sections with generally more superficial ingrowth in proximal parts of implant (ingrowth grades 1 or 3) than in distal parts (grades 0 and 1, see Table 3) in both animals (Figure 9C–F, Fig. 10C–F). More deep bone ingrowth was noticed in the most proximal implant section of animal 1 (grade 3) and in two most distal sections of animal 2 (grades 3 and 4, Table 3). The implant-skin-bone interface can be seen in longitudinal sections of Figure 9B and 10A, B. The epidermal layer enters the pores of both implants and extends into the deeper implant pores. Dermal ingrowth into the implant could be only assessed in animal 2 for technical reasons. Skin penetrated implant to depth of approximately 0.7 mm and followed the edge of the implant.

4. Discussion

4.1. Study objectives

The goal of the study was to develop a feline experimental model for detailed analysis of skin and bone integration with a porous titanium implant that is physiologically loaded during locomotion with DSA prostheses. The surgical, rehabilitation and recording procedures and prosthetic devices developed in this study allowed two experimental animals to adopt DSA prostheses for standing and locomotion for 11 weeks without clinical signs of infection, distress or pain. Full-body mechanical analysis of prosthetic gait revealed how the animals adapted to the prosthesis. Histological analysis of the porous titanium implants harvested at the end of the study demonstrated bone and skin ingrowth inside the implants. The obtained results confirmed our expectations about the use of DSA prostheses by the animal and tissue ingrowth into the implant.

4.2. Integration of porous titanium implant with the residual bone and skin

The findings of this study (Figures 1B, 3–10, Tables 1, 3) suggest that the porous titanium implants can serve as a reliable attachment point for an external prosthesis. Both implants demonstrated signs of integration with bone and one studied implant showed signs of integration with skin. There was at least mild bone growth into each quadrant of the proximal implant sections with more ingrowth seen in distal sections, which were in closer contact with the marrow cavity wall (Figure 1B). The skin ingrowth appeared to follow the implant into the distal end of the marrow canal. The lack of intimate bone-implant contact at the proximal end of the implant (about 1–3 cm from the implant exit point from tibia, Figures. 1B, 9A) might have been because the diameter of the distal end of the implant was smaller than the diameter of the bone canal. As a result, little or no bone ingrowth could be seen in those implant locations, which is expected. In some proximal implant locations, bone ingrowth into implant was evident without apparent implant contact with walls of the marrow canal (Figure 10C, D). This observation could be explained by possible bone ingrowth from a neighboring distal location of the implant, which was in contact with the tibia walls. Another explanation could be bone resorption near the proximal end of implant. Despite these effects, both animals demonstrated substantial loading of the prosthesis attached to the percutaneous implant during locomotion.

The obtained histological results are in agreement with previous studies that demonstrated bone and skin integration with similar porous titanium implants (Farrell et al., 2013b; Pitkin et al., 2007; Pitkin et al., 2009) or solid titanium implants coated with porous titanium (Isackson et al., 2011; Jeyapalina et al., 2012; Pendegrass et al., 2006b) in rats, a cat, rabbits, goats and sheep. Although osseointegration of solid titanium implants with bone has been well established in animal models and human patients (Branemark, 1983; Hagberg and Brånemark, 2009; Pitkin et al., 2007; Shelton et al., 2011; Ysander et al., 2001), skin integration with porous percutaneous implants has not been well documented. A limited number of studies have suggested the potential for these implants to form a skin barrier to pathogens at the skin-implant interface (Farrell et al., 2013b; Isackson et al., 2011; Jeyapalina et al., 2012; Pendegrass et al., 2006b; Pitkin et al., 2007). The results of this study support this suggestion.

An advantage of the animal model developed in this study compared to the majority animal models used previously is that it allows for an investigation of percutaneous implant properties after the animal has loaded it within physiological ranges during every day standing and locomotion with a prosthesis. Such a model is necessary for a meaningful translation of animal experimentation results to clinical studies and practice.

4.3. Prosthetic gait

Both implanted animals demonstrated stable prosthetic walking with normal speeds. As in another resent study of quadrupedal prosthetic locomotion in sheep (Shelton et al., 2011), the animals in our study loaded the prosthetic limb less than before surgery or than other intact limbs after surgery. The analysis of loads exerted by the contralateral fore- and hindlimb and the ipsilateral forelimb (Figures 6, 7) suggests that the animal shifted body weight (CoM) to the contralateral side. Left hindlimb increased its propulsive force, whereas the other two intact limbs decreased their breaking forces during prosthetic gait. This compensation strategy was employed by both animals and apparently helped the animals to maintain normal walking speed. Although the magnitude of unloading of the prosthetic limb is similar to the previous study on sheep (Shelton et al., 2011), the mechanism of this decrease seems different. In our study the ankle joint that provides a major contribution to energy generation for intact locomotion (Prilutsky et al., 1996; Prilutsky and Klishko, 2011; Prilutsky et al., 2011) was substituted with a passive prosthesis. In the sheep study, a much

smaller metacarpophalangeal joint was removed. We propose that the decrease in loading on the prosthetic limb in our study was a compensation strategy to allow the intact limbs to contribute more to propulsion. This explanation is supported by the greater magnitudes of the resultant muscle moments at joints of the intact limbs during prosthetic walking (Figure 8). In addition, the stance duration and duty factor of the intact limbs increased during prosthetic gait, apparently compensating for the deficits in the right hind prosthetic limb.

Acknowledgments

We thank the staff of St. Joseph's Translational Research Institute, especially Dr. Ashley Strong and Dr. Evan Goldberg for the excellent organization of animal care. We would also like to thank Alison Cerutti, BS for her assistance in determining the inertial properties of the prostheses and Ashley Heard, MS for her assistance in developing a feline prosthesis. The study was supported by NIH grants T32-HD055180-02 and R44HD057492 and by the Center for Human Movement Studies at Georgia Institute of Technology.

References

Aschoff HH, Juhnke DL. 10 Jahre endo-exo-femurprothetik zur rehabilitation nach oberschenkelamputation – Daten, fakten und ergebnisse. Zeitschrift fur Orthopadie und Unfallchirurgie. 2012; 150:607–614. [PubMed: 23171987]

Aschoff HH, Kennon RE, Keggi JM, Rubin LE. Transcutaneous, distal femoral, intramedullary attachment for above-the-knee prostheses: an endo-exo device. The Journal of bone and joint surgery. 2010; 92(Suppl 2):180–186. American volume. [PubMed: 21123601]

Barnett CT, Vanicek N, Polman RC. Postural responses during volitional and perturbed dynamic balance tasks in new lower limb amputees: a longitudinal study. Gait Posture. 2013; 37:319–325. [PubMed: 22921490]

Beloozerova IN, Farrell BJ, Sirota MG, Prilutsky BI. Differences in movement mechanics, electromyographic, and motor cortex activity between accurate and non-accurate stepping. Journal of neurophysiology. 2010; 103:2285–2300. [PubMed: 20164404]

Branemark PI. Osseointegration and its experimental background. Journal of Prosthetic Denistry. 1983; 50:399–410.

Brånemark R, Brånemark PI, Rydevik B, Myers RR. Osseointegration in skeletal reconstruction and rehabilitation: a review. Journal Of Rehabilitation Research And Development. 2001; 38:175–181. [PubMed: 11392650]

Brodell JD, Axon DL, Evarts CM. The Robert Jones bandage. Journal of bone and Joint Surgery. 1986; 68:776–779. [PubMed: 3782244]

Brown TG. On the Nature of the Fundamental Activity of the Nervous Centres. Journal of Physiology. 1914; 49:18–36. [PubMed: 16993247]

Buckley JG, O'Driscoll D, Bennet SJ. Postural sway and active balance performance in highly active lower-limb amputees. American Journal of Physical Medicine and Rehabilitation. 2002; 81:13–20. [PubMed: 11807327]

Chou TGR, Petti CA, Szakacs J, Bloebaum RD. Evaluating antimicrobials and implant materials for infection prevention around transcutaneous osseointegrated implants in a rabbit model. Journal of biomedical materials research Part A. 2010; 92:942–952. [PubMed: 19291687]

Curtze C, Hof AL, Postema K, Otten B. Over rough and smooth: amputee gait on an irregular surface. Gait Posture. 2011; 33:292–296. [PubMed: 21176879]

Curtze C, Hof AL, Postema K, Otten B. The relative contributions of the prosthetic and sound limb to balance control in unilateral transtibial amputees. Gait Posture. 2012; 36:276–281. [PubMed: 22525420]

D'Angeli V, Belvedere C, Ortolani M, Giannini S, Leardini A. Load along the femur shaft during activities of daily living. J Biomech. 2013; 46:2002–2010. [PubMed: 23845727]

Drillis R, Contini R, Bluestein M. Body segment parameters; a survey of measurement techniques. Artificial Limbs. 1964; 25:44–66. [PubMed: 14208177]

Drygas KA, Taylor R, Sidebotham CG, Hugate RR, McAlexander H. Transcutaneous tibial implants: a surgical procedure for restoring ambulation after amputation of the distal aspect of the tibia in a dog. Veterinary surgery: VS. 2008; 37:322–327. [PubMed: 18564255]

Farrell, BJ.; Kistenberg, RS.; Dalton, JF.; Strong, A.; Pitkin, M.; Prilutsky, BI. Evaluation of skin and bone integration with a porous titanium pylon after prosthetic gait rehabilitation in the cat. 4th International Conference: Advances in Orthopaedic Osseointegration; San Francisco, CA. 2012.

Farrell, BJ.; Prilutsky, BI.; Kistenberg, RS.; Dalton, JF., IV; Strong, A.; Pitkin, M. An animal model to study skin-implant-bone integration and prosthetic gait with limb prostheses directly attached to the residual limb. XXIV Congress of International Society of Biomechanics; Natal, Brazil. 2013a.

Farrell BJ, Prilutsky BI, Ritter JM, Kelley S, Popat KC, Pitkin M. Effects of pore size, implantation time and nano-surface properties on rat skin ingrowth into percutaneous porous titanium implants. Journal of biomedical materials research. Part A. 2013b May 23. Epub ahead of print. 10.1002/jbm.a.34807

Fernie GR, Kostuik JP, Lobb RJ. A percutaneous implant using a porous metal surface coating for adhesion to bone and a velour covering for soft tissue attachment: results of trials in pigs. Journal of biomedical materials research. 1977; 11:883–891. [PubMed: 145440]

Frossard L, Gow DL, Hagberg K, Cairns N, Contoyannis B, Gray S, Branemark R, Pearcy M. Apparatus for monitoring load bearing rehabilitation exercises of a transfemoral amputee fitted with an osseointegrated fixation: a proof-of-concept study. Gait Posture. 2010a; 31:223–228. [PubMed: 19926285]

Frossard L, Hagberg K, Häggström E, Brånemark R. Load-relief of walking AIDS on osseointegrated fixation: instrument for evidence-based practice. IEEE transactions on neural systems and rehabilitation engineering: a publication of the IEEE Engineering in Medicine and Biology Society. 2009; 17:9–14. [PubMed: 19211318]

Frossard L, Hagberg K, Haggstrom E, Gow DL, Branemark R, Pearcy M. Functional outcome of transfemoral amputees fitted with an osseointegrated fixation: temporal gait characteristics. JPO Journal of Prosthetics and Orthotics. 2010b; 22:11–20.

Frossard L, Haggstrom E, Hagberg K, Branemark R. Load applied on bone-anchored transfemoral prosthesis: characterization of a prosthesis-a pilot study. J Rehabil Res Dev. 2013; 50:619–634. [PubMed: 24013910]

Frossard L, Stevenson N, Smeathers J, Häggström E, Hagberg K, Sullivan J, Ewins D, Gow DL, Gray S, Brånemark R. Monitoring of the load regime applied on the osseointegrated fixation of a transfemoral amputee: a tool for evidence-based practice. Prosthetics and orthotics international. 2008a; 32:68–78. [PubMed: 18330805]

Frossard L, Stevenson N, Smeathers J, Haggstrom E, Hagberg K, Sullivan J, Ewins D, Gow DL, Gray S, Branemark R. Monitoring of the load regime applied on the osseointegrated fixation of a transfemoral amputee: a tool for evidence-based practice. Prosthetics and orthotics international. 2008b; 32:68–78. [PubMed: 18330805]

Frossard LA. Load on osseointegrated fixation of a transfemoral amputee during a fall: Determination of the time and duration of descent. Prosthetics and orthotics international. 2010; 34:472–487. [PubMed: 20961183]

Frossard LA, Tranberg R, Haggstrom E, Pearcy M, Branemark R. Load on osseointegrated fixation of a transfemoral amputee during a fall: loading, descent, impact and recovery analysis. Prosthetics and orthotics international. 2010c; 34:85–97. [PubMed: 20196690]

Glencross DJ. Control of skilled movements. Psychological bulletin. 1977; 84:14–29. [PubMed: 403535]

Goslow GE Jr, Reinking RM, Stuart DG. The cat step cycle: hind limb joint angles and muscle lengths during unrestrained locomotion. J Morphol. 1973; 141:1–41. [PubMed: 4727469]

Gregor RJ, Smith DW, Prilutsky BI. Mechanics of slope walking in the cat: quantification of muscle load, length change, and ankle extensor EMG patterns. J Neurophysiol. 2006; 95:1397–1409. [PubMed: 16207777]

Hagberg K, Branemark R. One hundred patients treated with osseointegrated transfemoral amputation prostheses--rehabilitation perspective. J Rehabil Res Dev. 2009; 46:331–344. [PubMed: 19675986]

Hagberg K, Brånemark R. One hundred patients treated with osseointegrated transfemoral amputation prostheses—Rehabilitation perspective. Rehabilitation. 2009; 46:331–344.

Hagberg K, Häggström E, Uden M, Brånemark R. Socket versus bone-anchored trans-femoral prostheses: Hip range of motion and sitting comfort. Prosthetics and orthotics international. 2005; 29:153–163. [PubMed: 16281724]

Hall CW. Developing a permanently attached artificial limb. Bulletin of prosthetics research. 1974:144–157. [PubMed: 4462894]

Hof AL, van Bockel RM, Schoppen T, Postema K. Control of lateral balance in walking. Experimental findings in normal subjects and above-knee amputees. Gait & posture. 2007; 25:250–258. [PubMed: 16740390]

Honeycutt CF, Nichols TR. The decerebrate cat generates the essential features of the force constraint strategy. J Neurophysiol. 2010; 103:3266–3273. [PubMed: 20089811]

Hoy MG, Zernicke RF. Modulation of limb dynamics in the swing phase of locomotion. J Biomech. 1985; 18:49–60. [PubMed: 3980488]

Isackson D, McGill LD, Bachus KN. Percutaneous implants with porous titanium dermal barriers: an in vivo evaluation of infection risk. Med Eng Phys. 2011; 33:418–426. [PubMed: 21145778]

Jacobs R, Brånemark R, Olmarker K, Rydevik B, Van Steenberghe D, Brånemark PI. Evaluation of the psychophysical detection threshold level for vibrotactile and pressure stimulation of prosthetic limbs using bone anchorage or soft tissue support. Prosthetics and orthotics international. 2000; 24:133–142. [PubMed: 11061200]

Jansen JA, de Groot K. Guinea pig and rabbit model for the histological evaluation of permanent percutaneous implants. Biomaterials. 1988; 9:268–272. [PubMed: 3408800]

Jansen, Ja; Paquay, YG.; van der Waerden, JP. Tissue reaction to soft-tissue anchored percutaneous implants in rabbits. Journal of biomedical materials research. 1994; 28:1047–1054. [PubMed: 7814432]

Jeyapalina S, Beck JP, Bachus KN, Williams DL, Bloebaum RD. Efficacy of a porous-structures titanium subdermal barrier for preventing infection in percutaneous osseointegrated prostheses. Journal of Orthopaedic Research. 2012; 30:1304–1311. [PubMed: 22294380]

Jonsson S, Caine-Winterberger L, Branemark R. Osseointegration amputation prostheses on the upper limbs: methods, prosthetics and rehabilitation. Prosthetics and Orthotics International. 2011; 35:190–200. [PubMed: 21697201]

Lee WC, Frossard LA, Hagberg K, Haggstrom E, Branemark R, Evans JH, Pearcy MJ. Kinetics of transfemoral amputees with osseointegrated fixation performing common activities of daily living. Clin Biomech (Bristol, Avon). 2007; 22:665–673.

Lee WC, Frossard LA, Hagberg K, Haggstrom E, Gow DL, Gray S, Branemark R. Magnitude and variability of loading on the osseointegrated implant of transfemoral amputees during walking. Med Eng Phys. 2008; 30:825–833. [PubMed: 17977050]

Manter JT. The Dynamics of Quadrupedal Walking. Journal of Experimental Biology. 1938; 15:522–540.

Mooney V, Schwartz SA, Roth AM, Gorniowsky MJ. Percutaneous implant devices. Annals of biomedical engineering. 1977; 5:34–46. [PubMed: 851262]

Murphy EF. History and philosophy of attachment of prostheses to the musculo-skeletal system and of passage through the skin with inert materials. Journal of biomedical materials research. 1973; 7:275–295. [PubMed: 4577874]

Musienko P, Courtine G, Tibbs JE, Kilimnik V, Savochin A, Garfinkel A, Roy RR, Edgerton VR, Gerasimenko Y. Somatosensory control of balance during locomotion in decerebrated cat. J Neurophysiol. 2012; 107:2072–2082. [PubMed: 22236709]

Pendegrass CJ, Goodship AE, Blunn GW. Development of a soft tissue seal around bone-anchored transcutaneous amputation prostheses. Biomaterials. 2006a; 27:4183–4191. [PubMed: 16618500]

Pendegrass CJ, Goodship AE, Blunn GW. Development of a soft tissue seal around bone-anchored transcutaneous amputation prostheses. Biomaterials. 2006b; 27:4183–4191. [PubMed: 16618500]

Pendegrass CJ, Goodship AE, Price JS, Blunn GW. Nature's answer to breaching the skin barrier: an innovative development for amputees. Journal of anatomy. 2006c; 209:59–67. [PubMed: 16822270]

Pendegrass CJ, Gordon D, Middleton CA, Sun SNM, Blunn GW. Sealing the skin barrier around transcutaneous implants. Journal of Bone and Joint Surgery. 2008; 90B:114–121. [PubMed: 18160512]

Pezzin L. Use and satisfaction with prosthetic limb devices and related services. Archives of Physical Medicine and Rehabilitation. 2004; 85:723–729. [PubMed: 15129395]

Pitkin M. Design features of implants for direct skeletal attachment of limb prostheses. Journal of biomedical materials research Part A. 2013; 101:3339–3348. [PubMed: 23554122]

Pitkin, M.; Blinova, MI.; Yudintseva, NV.; Potokin, IL.; Raykhtsaum, G.; Pinaev, GP. Skin and bone integrated prosthetic technology. I. Characterization and morphology of human cells cultivated on titanium implants of different structures. 9th Russian National Congress “People and Health”; St. Petersburg, Russia. 2004.

Pitkin M, Pilling J, Raykhtsaum G. Mechanical properties of totally permeable titanium composite pylon for direct skeletal attachment. Journal of biomedical materials research Part B, Applied biomaterials. 2012; 100:993–999.

Pitkin, M.; Raykhtsaum, G. Skin integrated device. US patent. #8257435.. 2012.

Pitkin M, Raykhtsaum G, Galibin OV, Protasov MV, Chihovskaya JV, Belyaeva IG. Skin and bone integrated prosthetic pylon: A pilot animal study. J Rehabil Res Dev. 2006; 43:573. [PubMed: 17123195]

Pitkin M, Raykhtsaum G, Pilling J, Galibin OV, Protasov MV, Chihovskaya JV, Belyaeva IG, Blinova MI, Yudintseva NM, Potokin I, Pinaev GP, Moxson V, Duz V. Porous composite prosthetic pylon for integration with skin and bone. Journal of Rehabilitation Research and Development. 2007; 44:723–738. [PubMed: 17943684]

Pitkin M, Raykhtsaum G, Pilling J, Shukeylo Y, Moxson V, Duz V, Lewandowski J, Connolly R, Kistenberg RS, Dalton JF IV, Prilutsky BI, Jacobson S, Western C. Mathematical modeling and Mechanical and histopathological testing of porous prosthetic pylon for direct skeletal attachment. Journal of Rehabilitation Research & Development. 2009; 46:315–330. [PubMed: 19675985]

Prilutsky BI, Herzog W, Allinger TL. Mechanical power and work of cat soleus, gastrocnemius and plantaris muscles during locmotion: possible functioncal significance of muscle design and force patterns. Journal of Experimental Biology. 1996; 199:801–814. [PubMed: 8788087]

Prilutsky, BI.; Klishko, NA. Control of locomotion: Lessons from whole-body biomechanical analysis. In: Danion, F.; Latash, ML., editors. Motor control: Theories experiments and applications. Oxford University Press; Oxford: 2011. p. 197-218.

Prilutsky BI, Maas H, Bulgakova M, Hodson-Tole EF, Gregor RJ. Short-term motor compensations to denervation of feline soleus and lateral gastrocnemius result in preservation of ankle mechanical output during locomotion. Cells Tissues Organs. 2011; 193:310–324. [PubMed: 21411965]

Prilutsky BI, Sirota MG, Gregor RJ, Beloozerova IN. Quantification of motor cortex activity and full-body biomechanics during unconstrained locomotion. Journal of neurophysiology. 2005; 94:2959–2969. [PubMed: 15888524]

Rajan S. Skin and soft-tissue infections: classifying and treating a spectrum. Cleveland Clinic journal of medicine. 2012; 79:57–66. [PubMed: 22219235]

Rossignol S. Plasticity of connections underlying locomotor recovery after central and/or peripheral lesions in the adult mammalts. Philosophical transactions Royal Society London B Biol Sci. 2006; 361:1647–1671.

Saunders MM, Brecht JS, Verstraete MC, Kay DB, Njus GO. Lower limb direct skeletal attachment. A Yucatan micropig pilot study. Journal of investigative surgery: the official journal of the Academy of Surgical Research. 2012; 25:387–397. [PubMed: 23215796]

Segal AD, Orendurff MS, Czerniecki J, Shofer JB, Klute GK. Local dynamic stability of amputees wearing a torsion adapter compared to a rigid adapter during straight-line and turning gait. Journal of Biomechanics. 2010; 43:2798–2803. [PubMed: 20719315]

Shelton TJ, Beck JP, Bloebaum RD, Bachus KN. Percutaneous osseointegrated prostheses for amputees: Limb compensation in a 12-month ovine model. Journal of Biomechanics. 2011; 44:2601–2606. [PubMed: 21920525]

Sherrington CS. Flexion-reflex of the limb, crossed extension-reflex, and reflex stepping and standing. J Physiol. 1910; 40:28–121. [PubMed: 16993027]

Shik ML, Severin FV, Orlovskii GN. Control of walking and running by means of electric stimulation of the midbrain. Biofizika. 1966; 11:659–666. [PubMed: 6000625]

Sullivan J, Uden M, Robinson KP, Sooriakumaran S. Rehabilitation of the trans-femoral amputee with an osseointegrated prosthesis: the United Kingdom experience. Prosthetics and orthotics international. 2003; 27:114–120. [PubMed: 14571941]

Tillander J, Hagberg K, Hagberg L, Brånemark R. Osseointegrated titanium implants for limb prostheses attachments: infectious complications. Clinical orthopaedics and related research. 2010; 468:2781–2788. [PubMed: 20473597]

Torcasio A, van Lenthe GH, Van Oosterwyck H. The importance of loading frequency, rate and vibration for enhancing bone adaptation and implant osseointegration. European cells & materials. 2008; 16:56–68. [PubMed: 19040192]

Tranberg R, Zugner R, Karrholm J. Improvements in hip- and pelvic motion for patients with osseointegrated trans-femoral prostheses. Gait Posture. 2011; 33:165–168. [PubMed: 21130654]

Van de Meent H, Hopman MT, Frolke JP. Walking ability and quality of life in subjects with transfemoral amputation: a comparison of osseointegration with socket prostheses. Arch Phys Med Rehabil. 2013; 94:2174–2178. [PubMed: 23774380]

Williams DL, Bloebaum RD, Beck JP, Petti CA. Characterization of bacterial isolates collected from a sheep model of osseointegration. Current Microbiology. 2010; 61:574–583. [PubMed: 20458482]

Ysander M, Brånemark R, Olmarker K, Myers RR. Intramedullary osseointegration: development of a rodent model and study of histology and neuropeptide changes around titanium implants. J Rehabil Res Dev. 2001; 38:183–190. [PubMed: 11392651]

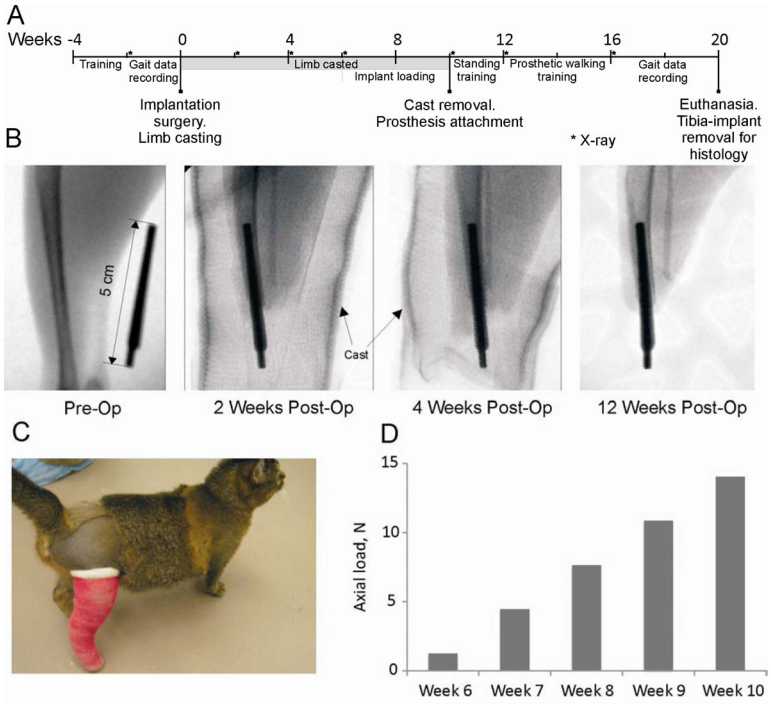

Figure 1.

Major stages of the study. A: Study timeline. Week 0 corresponds to the implantation surgery; the study ended with euthanasia and harvesting the residual limb with implant for histology (Week 21). B: X-ray images taken before surgery (Pre-Op), and 2, 4 and 12 weeks after implantation (Post-Op). C: Animal wearing a cast after pylon implantation to prevent premature loading of implant. D: Loads applied to implant using a handheld digital dynamometer from 6 to 10 weeks after implantation.

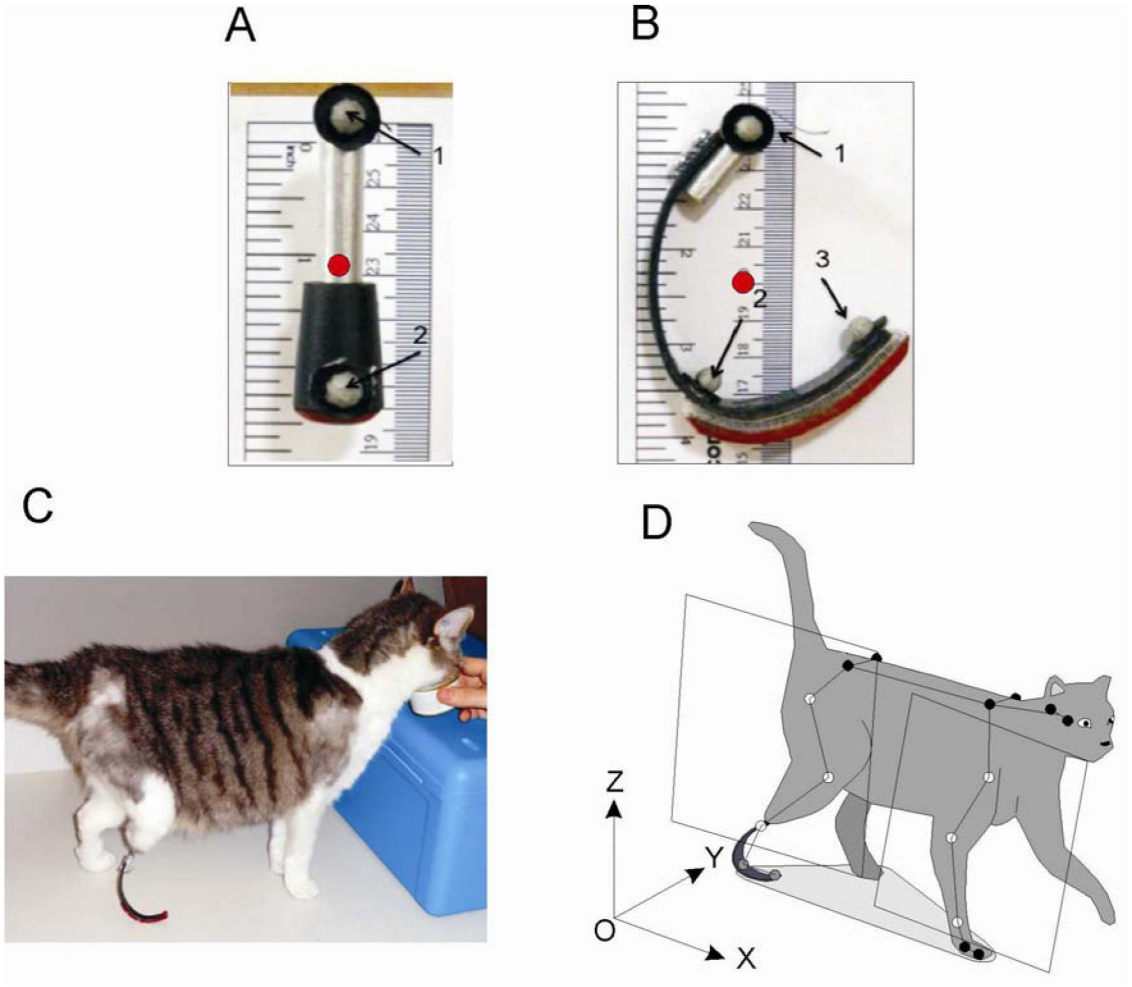

Figure 2.
Prosthetic design and cat model for motion analysis. A, B: Standing and walking prosthesis, respectively. Gray circles indicate marker placement on prostheses (marker 1 approximates location of the ankle center in the intact leg; marker 2, MTP joint; and marker 3, tip of the 5th digit). Red circles indicate center of mass of prosthesis. C: Standing on a walking prosthesis. D: A full-body cat model for motion analysis. The limb plane was defined for hind- and forelimbs using 3 markers on each limb (open markers; see text for further explanations).

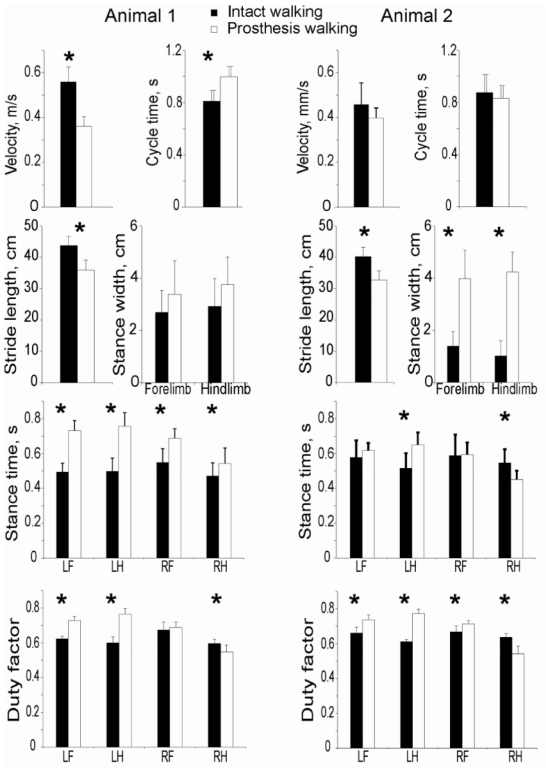

Figure 3.

Stride parameters (mean(SD)) of intact (filled bars) and prosthetic (unfilled bars) gait for cat 1 (left panels) and cat 2 (right panels). LF, LH, RF, and RH are left forelimb, left hindlimb, right forelimb, and right hindlimb, respectively; RH was implanted and had a DSA prosthesis on. Duty factor is the ratio of stance time and cycle time. * indicates significant differences between intact and prosthetic conditions ($P < 0.05$).

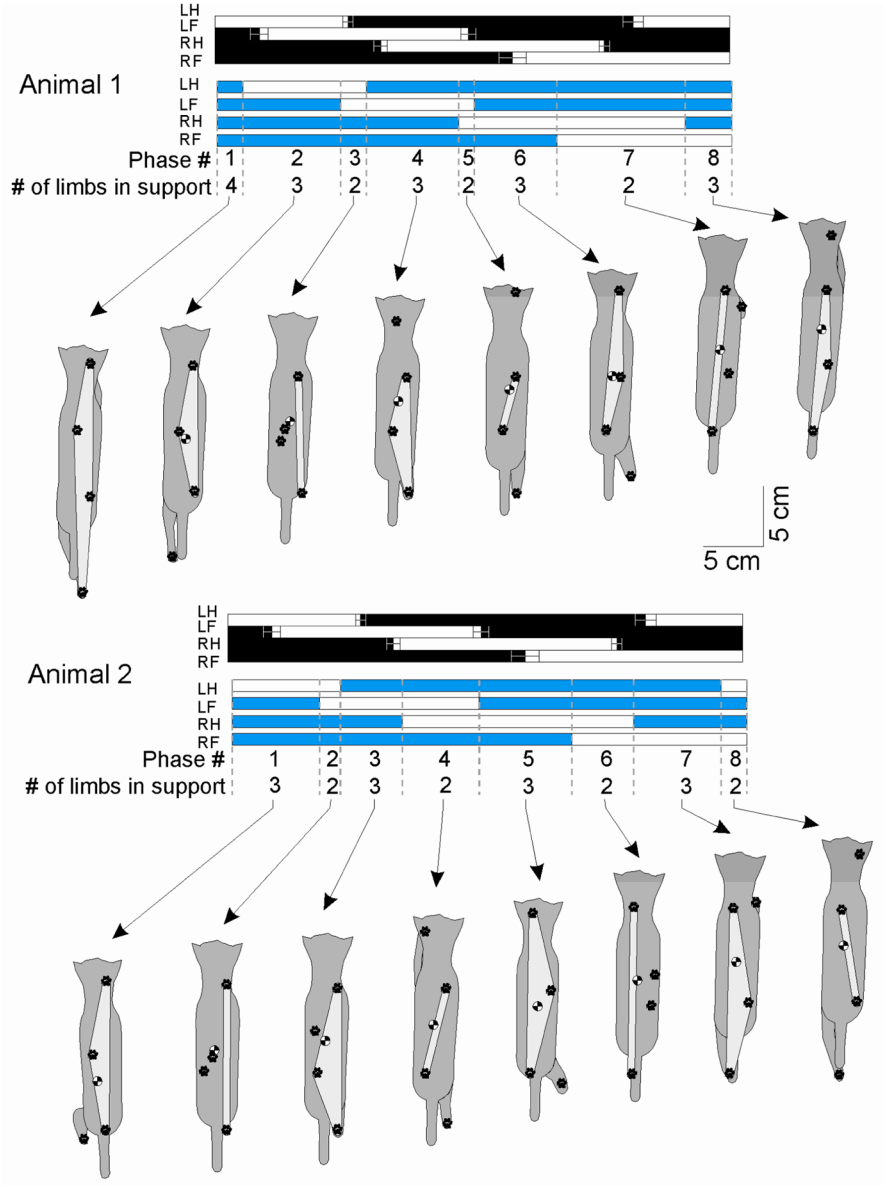

Figure 4.

Support pattern (sequence of phases with different number of limbs on the ground) during intact (black horizontal bars) and prosthetic (blue horizontal bars) walking and representative positions of two animals in each support phase. Filled bars indicate stance and unfilled bars swing. LH, LF, RH and RF are left hindlimb, left forelimb, right (prosthetic) hindlimb and right forelimb, respectively. The top row of numbers between dashed vertical lines indicate the phase of gait; the second row, the number of limbs on the ground in a given phase. Dorsal cat views show the base of support area (light gray) relative to the paws on the ground and the center of mass.

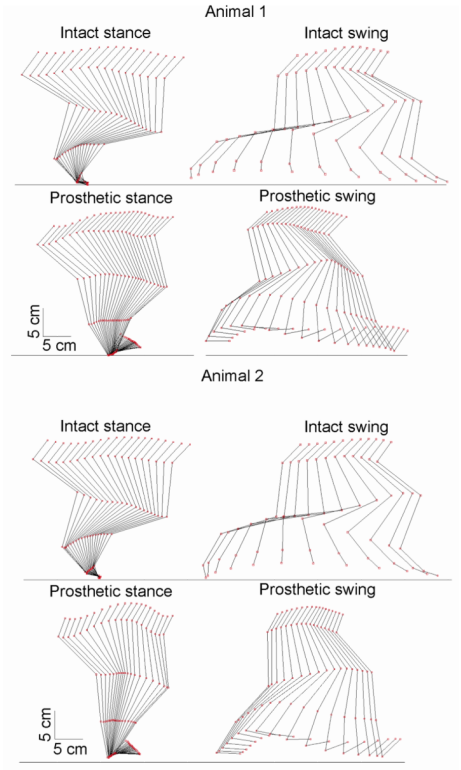

Figure 5.
Stick figures of the right hindlimb from representative trials of animal 1 (top 4 panels) and animal 2 (bottom 4 panels) during intact and prosthetic walking. Stance and swing phases are shown separately. Red squares represent the marker locations.

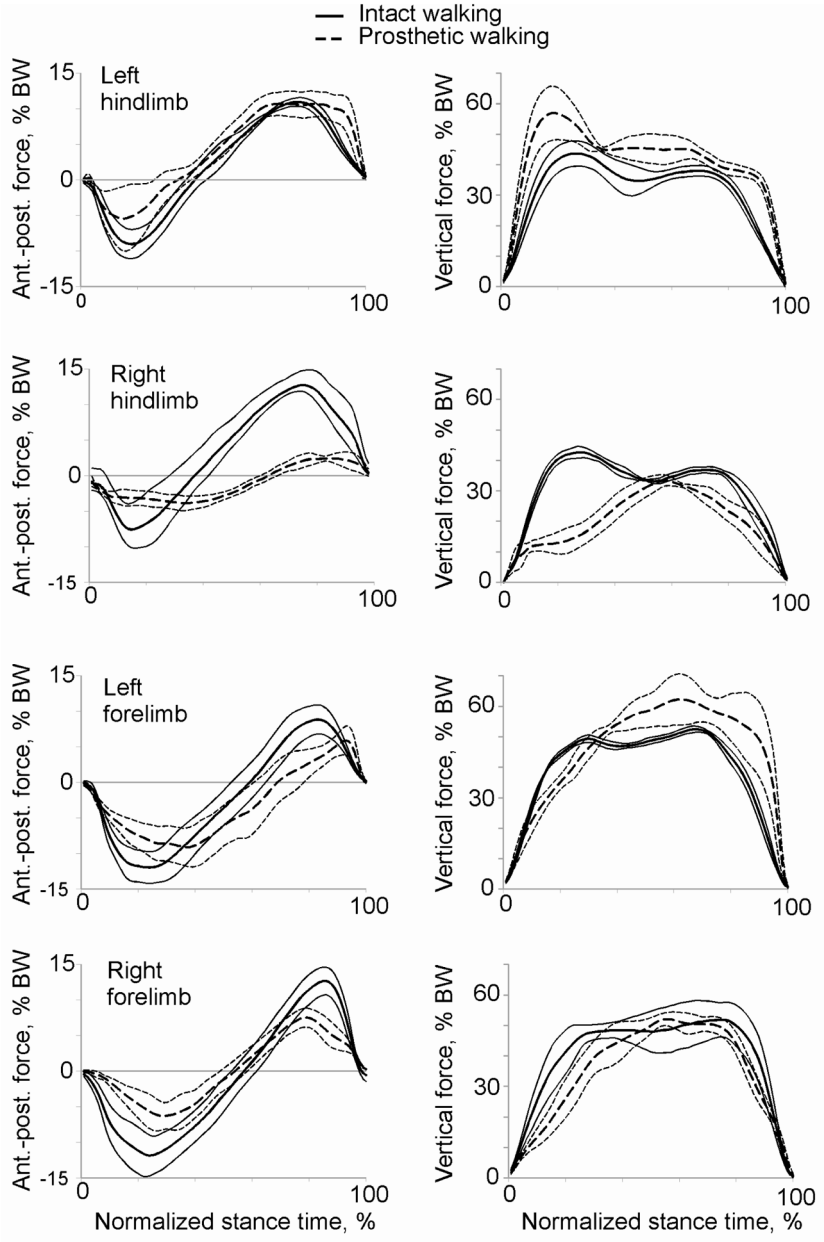

Figure 6.

Mean anterior-posterior (left) and vertical (right) ground reaction forces acting on individual limbs of cat 1 during intact (continuous lines) and prosthetic (dashed lines) gait conditions. Thin lines indicate SD. N = 6 – 7.

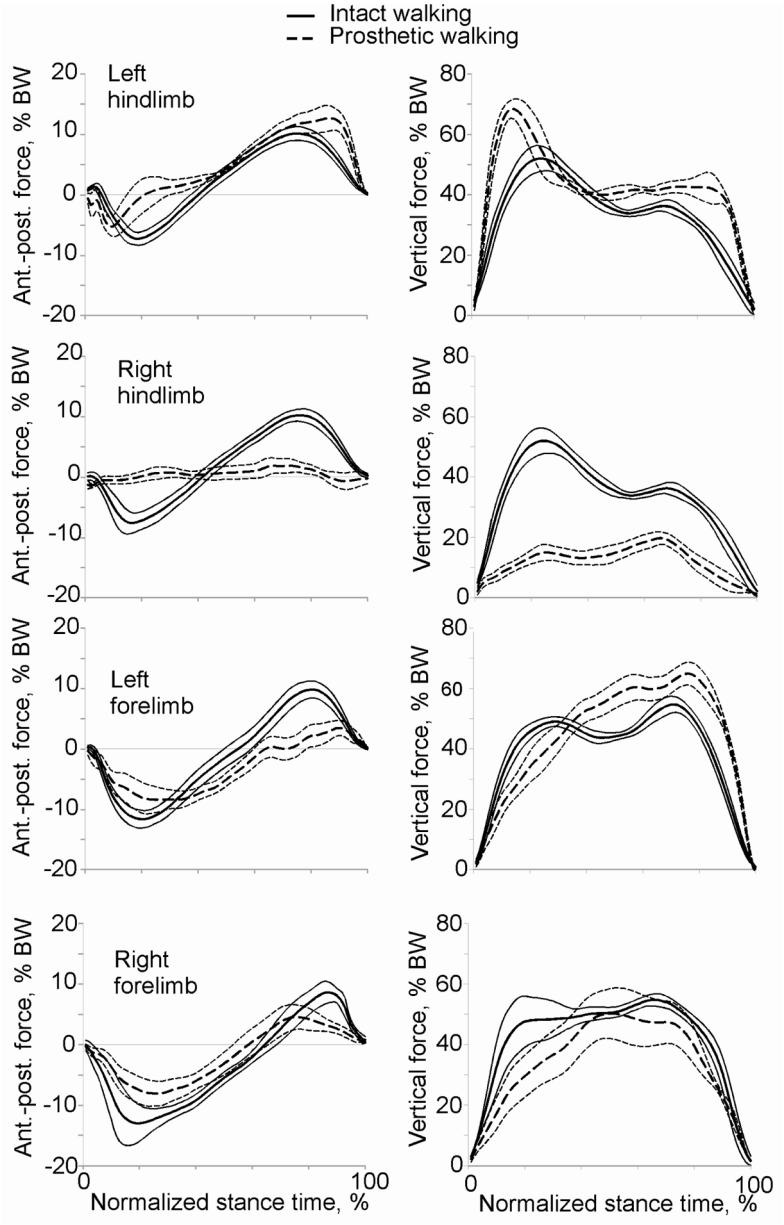

Figure 7.

Mean anterior-posterior (left) and vertical (right) ground reaction forces acting on individual limbs of cat 2 during intact (continuous lines) and prosthetic (dashed lines) gait conditions. Thin lines indicate SD. N = 6 – 8.

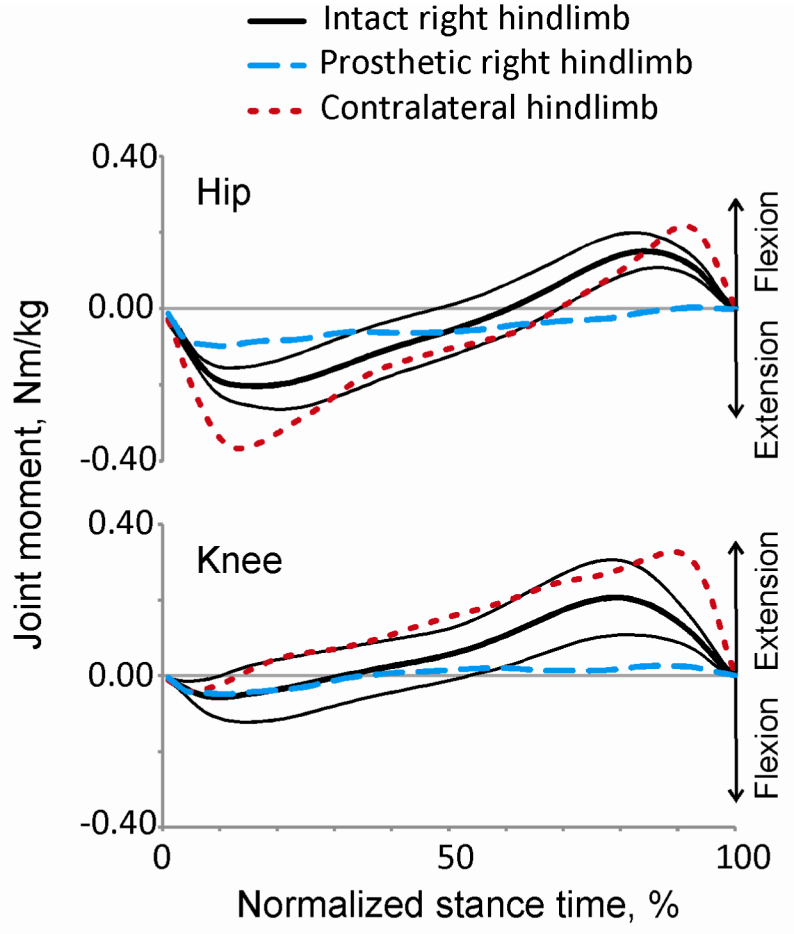

Figure 8.
Mean resultant muscle moments at the hip and knee joints of the ipsilateral and contralateral hindlimbs during stance of intact and prosthetic walking. Continuous lines are moments (mean(SD)) of the ipsilateral (right) hindlimb before surgery; dashed lines are mean moments of the prosthetic (ipsilateral) hindlimb; dotted lines are mean moments of the contralateral (left) hindlimb after surgery.

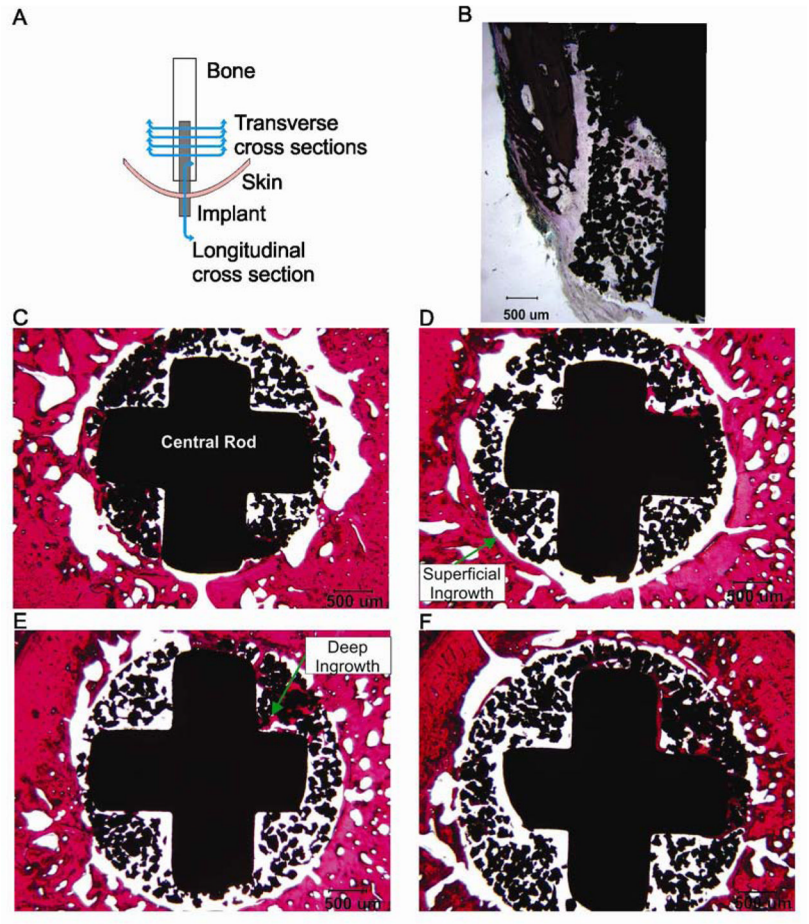

Figure 9.

Images of sections through implant, bone and skin from cat 1. Haemotoxylin and eosin staining. A: Schematics of the locations of the transverse and longitudinal sections of the implant. B: Longitudinal section through the distal implant (20x magnification). C–F: Transverse cross sections through the bone and implant from proximal to distal sections, respectively (20x magnification).

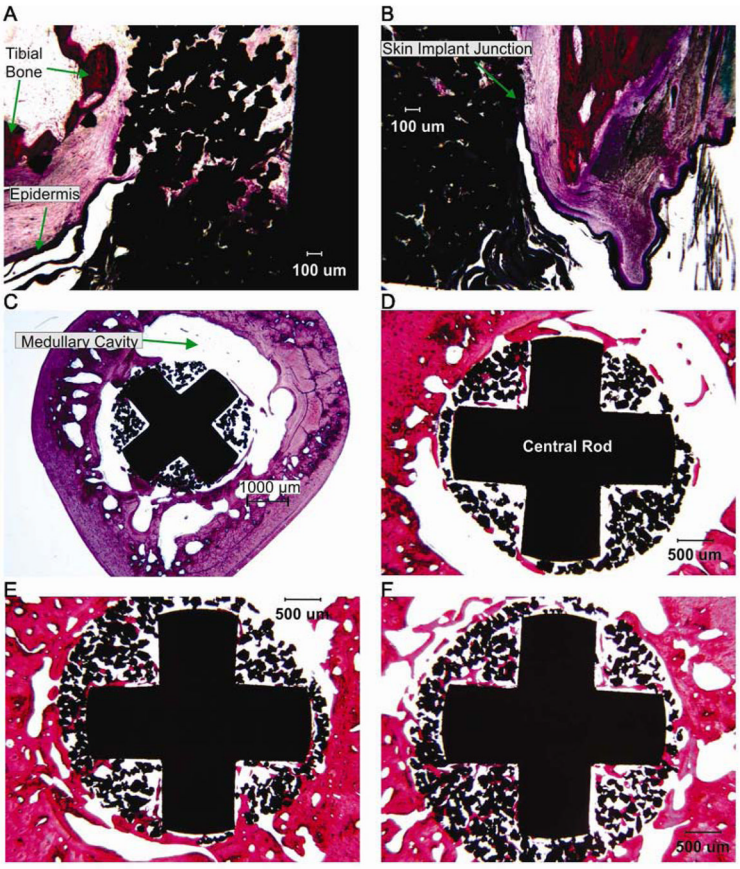

Figure 10.
Images of sections through implant, bone and skin from cat 2 (haemotoxylin and eosin stain). Locations of sections are shown in Fig. 9 A. A, B: Left and right views of the longitudinal section through the distal implant (40x magnification). C–F: Transverse cross sections through the bone and implant from proximal to distal sections, respectively (20x magnification).

Table 1

Cat and prosthesis biomechanical characteristics

Characteristics	Animal 1	Animal 2
Body mass		
Pre implantation body mass, kg	3.2	3.0
Post implantation body mass, kg	4.0	4.0
Segment length		
Thigh length, cm	9.8	9.8
Shank length, cm	10.5	10.4
Tarsals length, cm	5.6	6.2
Hind digits length, cm	3.2	3.8
Upper arm length, cm	8.4	9.0
Forearm length, cm	7.6	8.3
Carpals length, cm	2.4	2.2
Fore digits length, cm	3.4	3.2
Residual shank length, cm	8.5	8.8
Inertial properties of prosthesis		
Standing prosthesis mass, g	14.0 (20%)	14.0 (20%)
Standing prosthesis MOI, gcm^2	48.0 (20%)	48.0 (20%)
Walking prosthesis mass, g	18.4 (26%)	15.5 (22%)
Walking prosthesis MOI, gcm^2	157 (64%)	172 (71%)

Leg length was determined as the sum of thigh, shank and tarsals for the hindlimb and upper arm, forearm and carpals for the forelimb. MOI is moment of inertia with respect to the frontal axis through the center of mass. Numbers in parentheses indicate percentage of prosthesis mass and moment of inertia with respect to the estimated value of the corresponding hindlimb segments before surgery.

Table 2

Durations of phases (mean (SD)) in the limb support diagrams (Fig. 4). The total duration of 3–4 legged support was computed as the sum of durations of all phases with 3 or 4 legs in support.

Cat-1

Phase	Intact (% Cycle (SD))	Prosthesis (% Cycle (SD))
1	9.8 (1.9)	6.1 (2.9) *
2	19.0 (3.4)	16.9 (2.3)
3	9.6 (2.9)	6.9 (3.4)
4	13.4 (2.6)	17.1 (2.5) *
5	10.2 (1.1)	3.0 (2.1) *
6	14.2 (2.7)	16.7 (2.1)
7	10.2 (1.1)	24.6 (3.9) *
8	11.8 (2.8)	6.7 (4.5) *
3–4 legged support	39.8 ± 3.2	63.6 ± 6.1 *

Cat-2

Phase	Intact	Prosthesis
1	14.5 (7.2)	18.7 (3.1)
2	14.0 (3.3)	3.1 (1.9) *
3	11.4 (3.1)	12.1 (3.2)
4	8.4 (4.8)	14.0 (3.8) *
5	14.3 (3.4)	18.8 (2.3) *
6	14.8 (3.4)	12.0 (2.0)
7	12.5 (2.2)	16.1 (1.8) *
8	8.3 (3.0)	3.2 (1.8) *
3-legged support	52.63 (13.64)	65.58 (5.26) *

* Statistically different from the pre-implantation condition ($P<0.05$).

Table 3

Summary of histologic observations. Proximal sections of the tibia (I, II, III and IV) correspond to 4 transverse sections at the proximal half of implant from proximal end toward distal with a step of 2 mm; distal level corresponds to longitudinal section at the distal part of implant (see Fig. 9 A). Grades 1 through 4 were assigned in accordance with bone ingrowth in to one, two, three or four quadrants of the porous coating (Figs. 9 and 10). The distal longitudinal section for animal 1 could not be obtained and analyzed because of technical reasons.

Animal 1				
Level of the tibia	**Superficial ingrowth**	**Deep ingrowth**	**Impression of endosteal bone proliferation**	**Impression of periosteal bone proliferation**
Proximal I (nearest to the knee joint)	1	3	Mild	Minimal
Proximal II	3	1	Mild	Mild
Proximal III	3	1	Mild	Mild
Proximal IV (nearest to the amputation site)	1	1	Mild	Mild
Distal	N/A		N/A	N/A
Animal 2				
Proximal I (nearest to the knee joint)	3	1	Minimal to mild	Minimal
Proximal II	3	1	Mild	Mild
Proximal III	1	3	Mild to moderate	Moderate
Proximal IV (nearest to the amputation site)	0	4	Mild to moderate	Moderate to marked
Distal	1	3	Mild	Marked